JOURNAL OF Materials CHEMISTRY

Experimental and theoretical studies into the structural perturbations between neutral, oxidised and reduced forms of 1,4-dithiinoquinoxaline derivatives

Peter J. Skabara,*†[a] Rory Berridge,[a] Karen Prescott,[a] Leonid M. Goldenberg,‡[b] Enrique Ortí,[c] Rafael Viruela,[c] Rosendo Pou-Amérigo,[c] Andrei S. Batsanov,[d] Judith A. K. Howard,[d] Simon J. Coles[e] and Michael B. Hursthouse[e]

[a]*Division of Chemistry, Sheffield Hallam University, Sheffield, S1 1WB, UK. E-mail: P.J.Skabara@man.ac.uk*
[b]*Institute of Problems of Chemical Physics, Russian Academy of Science, Chernogolovka, 142432, Russia*
[c]*Department of Physical Chemistry, University of Valencia, Valencia, 46100, Spain*
[d]*Department of Chemistry, University of Durham, Durham, DH1 3LE, UK*
[e]*Department of Chemistry, University of Southampton, Southampton, SO17 1BJ, UK*

Received 16th May 2000, Accepted 21st July 2000
First published as an Advance Article on the web 27th September 2000

The syntheses and electrochemistry of thieno[3′,4′ : 5,6][1,4]dithiino[2,3-*b*]quinoxaline (**9**), 2,3-bis(methylsulfanyl)[1,4]dithiino[2,3-*b*]quinoxaline (**16**) and 2,3-ethylenedisulfanyl[1,4]dithiino[2,3-*b*]quinoxaline (**17**) are reported, together with the X-ray crystal structures of **9**, **16** and the charge-transfer complex **9**·TCNQ. In the thieno derivative **9**, the molecular structure undergoes a significant change from a boat conformer to a planar system, upon oxidation with TCNQ. Theoretical calculations show that oxidation leads to planarisation of the molecular structure due to the aromatisation of the dithiine moiety. The study of the oxidised/reduced species helps to rationalise the electrochemical behaviour observed experimentally.

The last quarter of this century has seen a growing interest in the preparation and characterisation of charge transfer (CT) complexes and salts based on organic electron donor and/or acceptor molecules. These materials have demonstrated fascinating electronic and magnetic properties, however, the bulk of research in this discipline has concentrated mainly on the conducting abilities of these species. There are numerous examples of CT salts representing semiconductors, organic metals and superconductors. In the latter case, the field is vastly dominated by materials comprising metal(dmit)$_2$ complexes (dmit = dimercaptoisotrithione or 1,3-dithiole-2-thione-4,5-dithiolate), tetrathiafulvalenes (TTF), tetraselenafulvalenes (TSF) and C_{60}.[1] The intense level of research in this area has been perpetuated by the drive to raise the T_c (temperature at which the onset of superconductivity occurs) of CT materials. However, there is still a need for the synthesis of new classes of donor or acceptor systems to build upon our understanding of CT complexes,[2] particularly since there is a growing number of applications for these types of materials, which detract from the original and exclusive theme of electrical conducting properties.[3]

Recently, several groups have been investigating the electron donor ability of polyheterocyclic systems incorporating fused 1,4-dithiine units. Some interesting examples include the tetrathiafulvalene derivatives **1**[4] and **2**,[5] acenaphthenes **3**,[6] **4**[6] and **5**,[7] tetraalkoxydibenzothianthrene **6**,[8] dithiinodiquinoxaline **7**[8] and the tetramethoxybenzodithiinopyridine **8**.[9] An appealing feature of compounds such as **1**–**8** centres on the non-planar contribution of the 1,4-dithiine species (the molecules usually adopt a boat conformation of the 1,4-dithiine ring with folding along the S···S vector).[10] In many superconducting CT complexes the donor domain constitutes dimers of neutral and oxidised molecules (DD^+ or D_2^+). From *ab initio* quantum mechanical calculations,[11] it has been shown that organic superconductors based on TTF or TSF contain folded donor (D) molecules and planar oxidised donor (D^+) species, leading to a relationship between charge transfer and deformation phonon modes; this relationship is believed to be responsible for superconductivity. Organic electron donor systems incorporating the 1,4-dithiine unit are, therefore, interesting candidates as components in potentially superconducting CT materials.

Results

Synthesis

We have prepared a fused thienodithiinoquinoxaline derivative (**9**), representing a new polyheterocyclic donor system with pronounced non-planar character in the neutral state. The synthesis of **9** was achieved by the reaction of thieno[3,4-*d*]-[1,3]dithiol-2-one (**10**)[12] with sodium ethoxide (generating the dithiolate intermediate **11**), followed by the addition of 2,3-dichloroquinoxaline (Scheme 1, 42% yield). Using exactly the same methodology, the dithiinoquinoxaline derivatives **16** and **17** were prepared from the dithiolate salts **14** and **15**, which were prepared *in situ via* the corresponding [1,3]dithiol-2-one compounds **12**[13] and **13**[13] (55% and 48% yield, respectively).

Complexation of **9** with the electron acceptor tetracyano-*p*-quinodimethane (TCNQ), in acetonitrile, afforded a dark green crystalline material. Although CHN analysis showed that the bulk material represented a stoichiometry of 3 : 1 (**9**·TCNQ), all the well-formed crystals proved to be a 1 : 1 complex **9**·TCNQ, as confirmed by X-ray analysis.

†Present address: Department of Chemistry, University of Manchester, Manchester, UK.
‡Present address: Institute of Thin Film Technology and Microsensorics, Berlin, Germany.

 DOI: 10.1039/b003910l

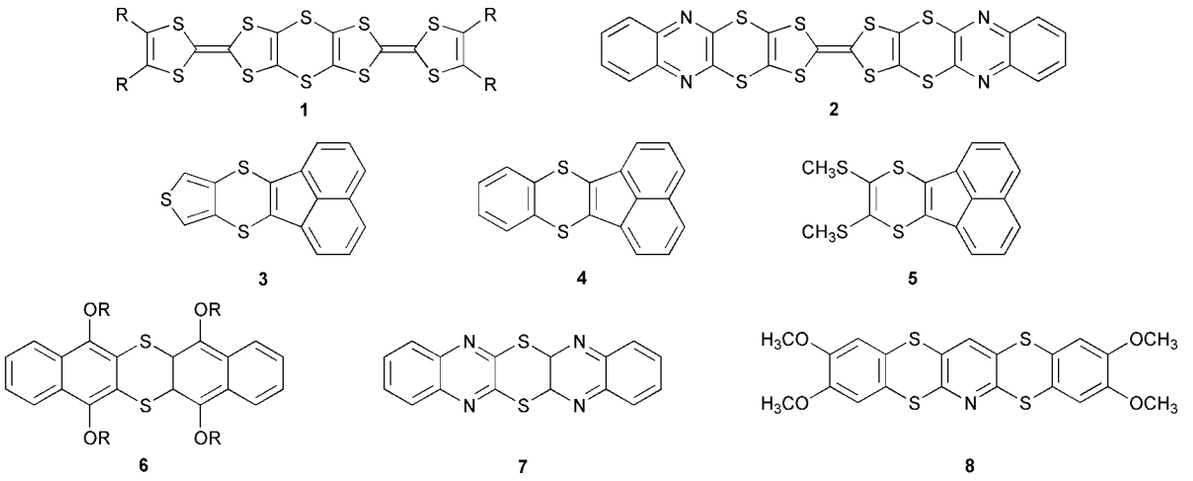

Electrochemistry

The electrochemical behaviour of the three dithiinoquinoxaline derivatives are remarkably different. The cyclic voltammogram of compound **9** is shown in Fig. 1, and demonstrates the typical amphoteric redox nature of the dithiinoquinoxaline derivatives (*i.e.* the ability to undergo both oxidation and reduction). Two oxidation peaks are observed at *ca.* +1.6 V and +2.0 V, representing the formation of the radical cation $\mathbf{9}^{+\bullet}$ and dication $\mathbf{9}^{2+}$, respectively. The oxidation peaks are irreversible, due to the instability and subsequent reactivity of the charged intermediates. The main reaction is the dimerisation of the radical cation $\mathbf{9}^{+\bullet}$, leading eventually to the formation of poly(**9**).[14] Three reduction peaks of different intensity (A, B and C in Fig. 1) can be seen during the reverse scan. Peak B at *ca.* 0.0 V probably corresponds to the reduction of cleaved protons.[15] When the experiment is limited to an upper value of +1.7 V, peaks A and C disappear, indicating that these two processes are connected to some by-product obtained from the unstable dication species $\mathbf{9}^{2+}$.

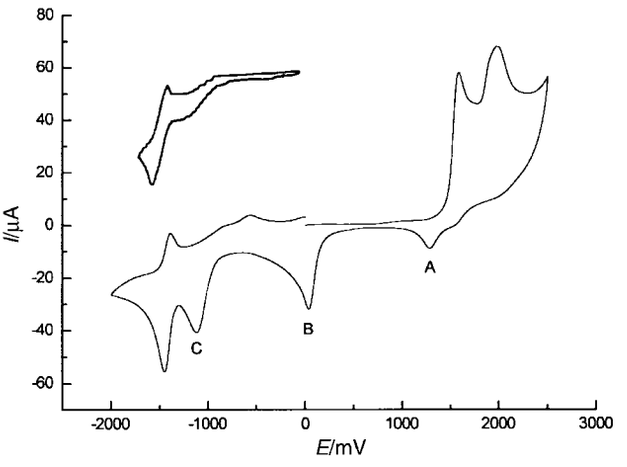

Fig. 1 Cyclic voltammogram of compound **9** *vs.* Ag/AgCl, Pt electrode, 20 °C, under argon, *ca.* 0.1 M $TBAPF_6$ supporting electrolyte, *ca.* 10^{-4} M substrate in dry dichloromethane, scan rate 200 mV s^{-1} with *iR* compensation. All waves represent single electron processes. Inset shows a negative scan from 0.0 V→−1.8 V→0.0 V.

The quasi-reversible single electron reductive wave at *ca.* −1.45 V is attributed to the quinoxaline moiety of compound **9**

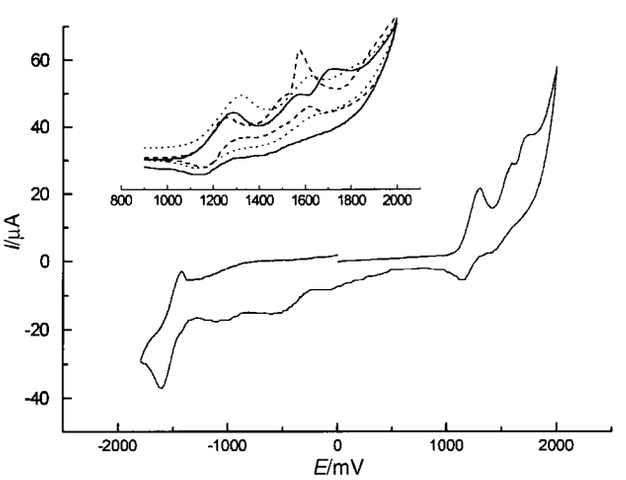

Fig. 2 Cyclic voltammogram of compound **16** (200 mV s^{-1}); inset (current in arbitrary units) shows the oxidation processes between 900 and 2000 mV at scan rates of 20 (- - -), 200 (—) and 600 mV s^{-1} (·····).

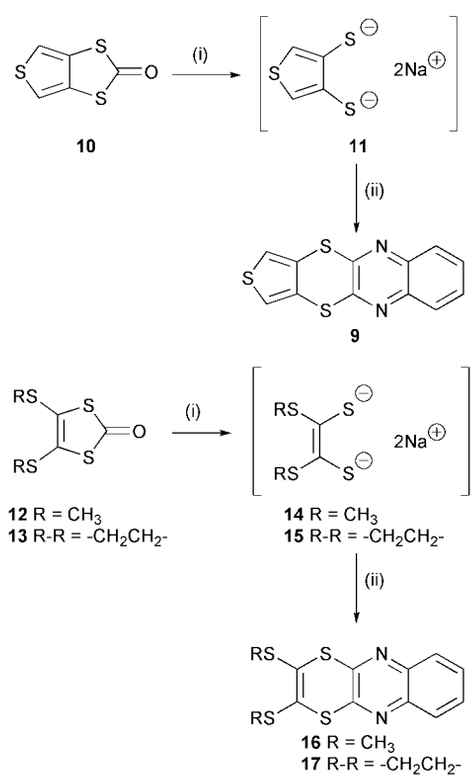

Scheme 1 *Reactions and conditions*: (i) NaOEt (2 equiv.), EtOH, 0 °C, 45 min; (ii) 2,3-dichloroquinoxaline, 20 °C, 16 h.

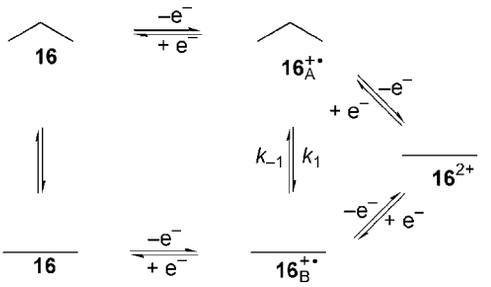

Fig. 3 Square scheme for the oxidation processes of compound **16**.

(quinoxaline itself is reduced at −1.80 V *vs.* Ag/AgCl in DMF).[16] An identical trace and potential value was observed by switching the experimental parameters from an initial positive sweep to negative, confirming that this redox process is not simply the reduction of a positively charged species (inset in Fig. 1).

The reversible reduction of the quinoxaline unit in **16** is clearly seen at −1.47 V (Fig. 2, 200 mV s^{-1}). The anodic electroactivity of derivative **16**, however, is highly dependent upon the scan rate. At 10 mV s^{-1}, two oxidation peaks are observed at *ca.* +1.2 V and +1.6 V, the latter being irreversible. Starting from 30 mV s^{-1}, the emergence of an additional quasi-reversible oxidation peak is seen at *ca.* +1.5 V. By increasing the scan rate, we observed the growth of this new redox process and the simultaneous disappearance of the original oxidation peak at +1.6 V. At a scan rate of 650 mV s^{-1}, the latter signal is finally lost. This type of behaviour can be explained if we assume that two conformers of the radical cation $\mathbf{16}^{+\bullet}$ participate in a square scheme, as depicted in Fig. 3. Upon loss of a single electron, the charged radical species converts from a nonplanar intermediate ($\mathbf{16}^{+\bullet}{}_{A}$) to a planar system ($\mathbf{16}^{+\bullet}{}_{B}$), in order to maximise π-orbital overlap in the pseudoaromatic 15 π-electron species. If we assume that the second oxidation process ($\mathbf{16}^{+\bullet}\rightarrow\mathbf{16}^{2+}$) rapidly affords a planar 14 π-electron aromatic dication, and the rate for the conversion $\mathbf{16}^{+\bullet}{}_{A}\rightarrow\mathbf{16}^{+\bullet}{}_{B}$ (k_1 in Fig. 3) is sufficient for the process to be observed by cyclic voltammetry, then the two oxidation peaks which are dependent upon the scan rate are probably representative of the electroactivity of the nonplanar and planar cation radicals (*i.e.* $\mathbf{16}^{+\bullet}{}_{A}\rightarrow\mathbf{16}^{2+}$ and $\mathbf{16}^{+\bullet}{}_{B}\rightarrow\mathbf{16}^{2+}$, respectively). The individual assignment of these processes to the second oxidation waves can be made on the assumption that the formation of a planar molecule is highly favoured. At slower scan rates (10–20 mV s^{-1}), the conversion of $\mathbf{16}^{+\bullet}{}_{A}$ to $\mathbf{16}^{+\bullet}{}_{B}$ is approximately at its equilibrium and is heavily biased towards the planar intermediate $\mathbf{16}^{+\bullet}{}_{B}$. Thus, the second oxidation potential at +1.6 V is due to the loss of an electron from the planar cation radical. As the scan rate of the experiment is increased, the concentration of the nonplanar species $\mathbf{16}^{+\bullet}{}_{A}$ increases and the new signal at +1.5 V represents the oxidation of this intermediate. The rationale behind the difference in oxidation potentials between $\mathbf{16}^{+\bullet}{}_{A}$ and $\mathbf{16}^{+\bullet}{}_{B}$ (*ca.* 80 mV) can be explained by the loss in driving force for the second oxidation in $\mathbf{16}^{+\bullet}{}_{B}$, since this intermediate has already reached planarity. It is noteworthy that the first oxidation becomes reversible when the upper limit of the scan is set to +1.45 V (observed at scan rates of 10, 100 and 1000 mV s^{-1}); however, the second oxidation potentials for the two conformers of the cation radical are too close together to assess any change in electrochemical behaviour by limiting the forward scan to a value of, for example, +1.60 V (*i.e.* half-way between E_{2ox} for $\mathbf{16}^{+\bullet}{}_{A}$ and that of $\mathbf{16}^{+\bullet}{}_{B}$).

The anodic behaviour of **16** can be attributed to the dithiine ring. In contrast, there are two possible sites of oxidation in compound **9**, *viz.* the 1,4-dithiine and thiophene sub-units.

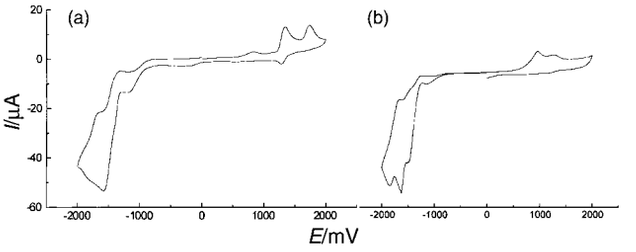

Fig. 4 Cyclic voltammogram of compound **17** (200 mV s^{-1}): (a) initial positive scan; (b) initial negative scan.

When the forward scan is confined to the first oxidation process (0 to +1.70 V), E_{1ox} remains irreversible (*cf.* the analogous reversible process observed in compound **16**). The appearance of a dark red film on the surface of the working electrode during continuous anodic scanning indicates the formation of a polymeric material.[14] Due to the well-known ability of thiophene derivatives to undergo electropolymerisation,[17] this suggests that E_{1ox} is due to the electroactivity of the thiophene unit. On varying the scan rate, the redox behaviour of **9** remains essentially unchanged.

The electrochemical behaviour of derivative **17** is particularly unusual (Fig. 4). From an initial positive scan, two weak, oxidation peaks are observed at *ca.* +1.4 and +1.7 V, whilst the cathodic sweep remains free from electroactivity in the range +2.00 to −1.20 V. Three reductive peaks (which were observed after deconvolution) occur at *ca.* −1.4 V (irreversible), −1.5 V (quasi-reversible) and −1.7 V (quasi-reversible), yet the number of electrons involved in these processes (three) does not correlate with a two electron process observed during oxidation, which would be predicted on the basis of the results from **9** and **16**. Notably, there is no change in the appearance or position of the oxidation peaks on variation of the scan rate and, more importantly, all three reductive peaks are observed when the CV experiment is initiated in a negative direction (0.00→−2.00 V→*etc.*), indicating that **17** behaves as a multi-acceptor species. Finally, it is worth noting that the oxidation peaks are shifted to lower values (*ca.* +0.96 and +1.28 V) when the scan is performed in the negative direction. This feature, together with the irreversibility of the reductive peaks, is indicative of side-reactions and the formation of side-products should be considered.

X-Ray crystallography

The asymmetric unit of **9** contains one molecule, shown in Fig. 5 (for bond distances, see Table 1). The molecular conformation can be roughly described as a folding by *ca.* 50.3° along the S(2)···S(3) vector into two planar moieties. However, while both the thiophene and the quinoxaline systems are rigorously planar, the S(2) and S(3) atoms tilt out of the quinoxaline plane by 0.20 and −0.03 Å and S(2) tilts also out of the thiophene plane by 0.05 Å. Thus the boat conformation of the dithiine ring is slightly twisted. The crystal packing (Fig. 6) is characterised by stacks of (crystallographically) parallel quinoxaline moieties, with alternating interplanar separations of 3.54 and 3.28 Å and lateral shifts between adjacent molecules of *ca.* 0.6 Å and 1.7 Å, respectively.

The asymmetric unit of **9**·TCNQ comprises two molecules of

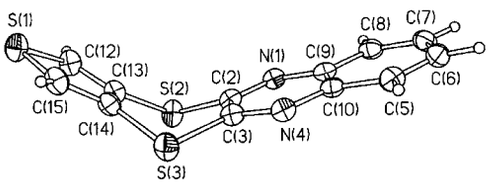

Fig. 5 Molecule in the crystal of **9**, showing 50% thermal ellipsoids.

Table 1 Selected experimental and calculated bond lengths (in Å) and folding angle (°)

			9·TCNQ[a]						
Bond	**9**[a]	**9**[b]	A	B	$\mathbf{9}^{+\bullet b}$	$\mathbf{9}^{2+bc}$	$\mathbf{9}^{2+bd}$	$\mathbf{9}^{-\bullet b}$	**16**[e]
S(1)–C(12)	1.721(2)	1.722	1.709(5)	1.702(5)	1.703	1.696	1.708	1.730	
C(12)–C(13)	1.360(3)	1.367	1.378(7)	1.368(5)	1.378	1.384	1.387	1.367	
C(13)–C(14)	1.430(3)	1.430	1.432(6)	1.451(6)	1.448	1.471	1.443	1.438	
S(2)–C(13)	1.764(2)	1.761	1.751(5)	1.751(5)	1.731	1.706	1.722	1.760	1.762(2)
S(2)–C(2)	1.777(2)	1.775	1.758(5)	1.759(5)	1.746	1.718	1.741	1.796	1.767(2)
C(2)–C(3)	1.444(3)	1.440	1.443(6)	1.444(6)	1.434	1.456	1.432	1.386	1.414(4)
N(1)–C(2)	1.308(3)	1.307	1.319(6)	1.323(6)	1.317	1.321	1.323	1.345	1.309(3)
N(1)–C(9)	1.373(3)	1.360	1.370(6)	1.363(6)	1.343	1.335	1.339	1.371	1.380(3)
C(9)–C(10)	1.421(3)	1.422	1.419(7)	1.426(7)	1.445	1.477	1.439	1.438	1.396(4)
C(8)–C(9)	1.416(3)	1.411	1.415(7)	1.412(7)	1.415	1.413	1.419	1.406	1.411(3)
C(7)–C(8)	1.369(3)	1.376	1.365(7)	1.381(7)	1.371	1.370	1.395	1.395	1.365(3)
C(6)–C(7)	1.420(3)	1.413	1.430(8)	1.420(8)	1.426	1.442	1.405	1.394	1.390(5)
Folding angle[f]	46.0	34.4	7.4	2.1	0.0	0.0	0.0	39.7	28.4(1)

[a]X-Ray data averaged over chemically equivalent bonds. [b]Minimum-energy B3P86/6-31G*-optimised structure. [c]Singlet state. [d]Triplet state. [e]X-Ray chemically equivalent bonds in **16** (atom numbering has been adapted to that used for **9**). All species have a mirror symmetry plane bisecting the molecule along the long molecular axis. [f]Angle formed by the planar units on both sides of the dithiine ring.

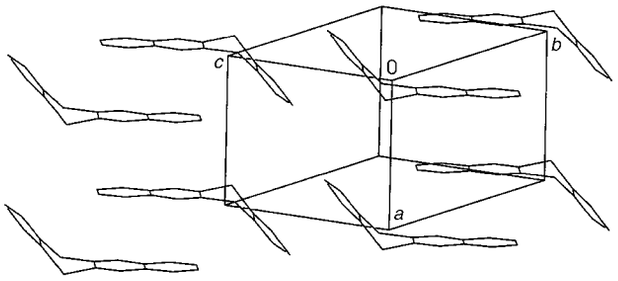

Fig. 6 Crystal structure of **9**, H atoms are omitted.

9 (*A* and *B*, see Fig. 7) and two of TCNQ (*C* and *D*). The dispersion of the lengths of chemically equivalent bonds does not exceed estimated standard deviations (esd's) of individual lengths, except for the C–N bonds of the TCNQ, where it equals 2 esd. Both donor molecules adopt a much more planar conformation than in the crystal of pure **9**, molecule *A* folding along the S(2)···S(3) vector by 8.5° and molecule *B* by only 1.7°. The bond distances in molecules *A* and *B* (Table 1) differ insignificantly, although consistently with a higher degree of π-delocalisation in the more planar *B*. In both TCNQ molecules, the $C(CN)_2$ moieties are tilted out of the ring plane in a boat fashion, by 4–5° in *C*, 1–4° in *D*. The donor and acceptor molecules are packed in mixed stacks $\cdot\cdot A\cdot\cdot C\cdot\cdot A\cdot\cdot C\cdot\cdot$ and $\cdot\cdot B\cdot\cdot D\cdot\cdot B\cdot\cdot D\cdot\cdot$ (Fig. 8); mean planes of adjacent molecules are essentially parallel with uniform interplanar separations of *ca.* 3.4 Å. Neither structure contains intermolecular contacts significantly shorter than the sums of van der Waals radii.[18]

Bond distances in TCNQ (see Table 2) give a reliable

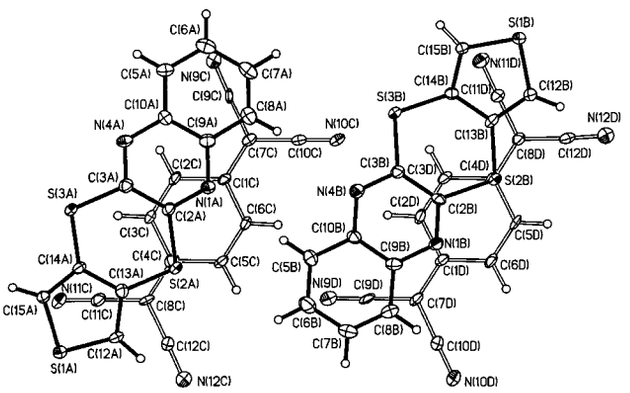

Fig. 7 Molecules in the crystal of **9**·TCNQ, showing 50% thermal ellipsoids.

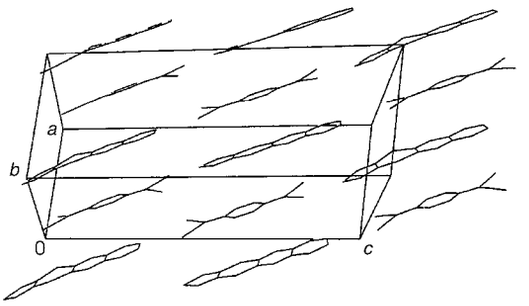

Fig. 8 Crystal packing of **9**·TCNQ, H atoms are omitted.

measure of charge transfer;[19,20] the *iii*−*ii* and *iii*−*iv* differences decrease linearly with the accumulation of negative charge, approaching $ii \approx iii \approx iv$ for a $TCNQ^-$ anion. Surprisingly, the (practically identical) geometry of both TCNQ moieties in the present complex shows only insignificant deviation from that of a neutral molecule.

The structure of **16** comprises one molecule in the asymmetric unit and is depicted in Fig. 9. The molecule is composed of three fused rings, where the quinoxaline moiety is planar and the dithiine ring is in an ideal boat conformation. The folding along the S(1)···S(1′) vector (40.5°) is significantly smaller than that found for **9** (50.3°). The difference is attributed to the out-of-plane disposition of the sulfanyl substituents, which interact with the quinoxaline moiety of an adjacent molecule in the crystal. Molecule **16** packs in an antiparallel assembly, where the aromatic rings are tilted away

Table 2 Mean bond lengths (Å) in TCNQ moieties

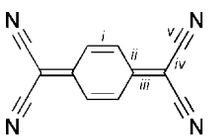

	$TCNQ^{0\,a}$	**9**·TCNQ[b]	$TCNQ^{-\bullet c}$
T/ K	100	120	110–178
i	1.354(1)	1.344(6)	1.362
ii	1.450(1)	1.448(6)	1.419
iii	1.382(1)	1.379(6)	1.417
iv	1.438(1)	1.438(7)	1.417
v	1.153(1)	1.145(8)	1.151

[a]A. S. Batsanov and J. A. K. Howard, unpublished data. [b]This work. [c]Average from 4 structures, ref. 20.

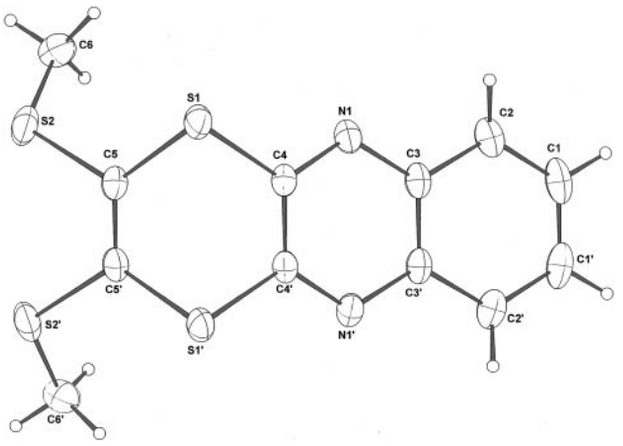

Fig. 9 Molecular structure of **16**, with ellipsoids at 50% probability.

from each other, reducing the π···π interaction (closest centroid–centroid separation = 4.257(13) Å). There are no further significant intermolecular interactions present.

Molecular orbital calculations

The molecular and electronic structures of compound **9**, its molecular constituents quinoxaline, 1,4-dithiine and thiophene and its bis(methylthio) (**16**) and ethylenedithio (**17**) analogues were theoretically investigated by using *ab initio* Hartree–Fock (HF) and density functional theory (DFT) calculations. The DFT approach has the advantage of including electron correlation effects and has been shown to provide more accurate molecular geometries. The discussion presented below thus relies mainly on DFT results. DFT calculations were performed using the B3P86 functional. The polarised 6-31G* basis set was used for both DFT and HF calculations. Single-point Møller–Plesset (MP2) calculations using DFT-optimised geometries were also carried out for compound **16**.

Neutral compounds. The molecular structure of compound **9** was optimised in both planar (C_{2v} symmetry) and nonplanar (C_s symmetry) conformations. The minimum-energy conformation corresponds to a folded C_s structure, similar to that found from X-ray analysis (Fig. 5), which is calculated to be 1.79 kcal mol^{-1} more stable than the planar C_{2v} structure at the B3P86/6-31G* level. This energy difference increases to 3.56 kcal mol^{-1} at the HF/6-31G* level. The folding angle of the dithiine ring has a value of 42.3° in good agreement with the X-ray value reported for 1,4-dithiine (43°),[21] but underestimating by 8.0° the average X-ray value observed for **9** (50.3°). This underestimation is in part due to the disposition of the molecules in the crystal (Fig. 6), for which packing forces favour more folded structures to achieve the most compact packing. As observed in the crystal, DFT calculations predict that the S(2) and S(3) atoms tilt out of the quinoxaline and thiophene planes by 0.19 and 0.05 Å, respectively. The angle formed by those planes (DFT: 34.3°; HF: 40.9°; X-ray: 46.0°) is, therefore, smaller than that corresponding to the folding of the dithiine moiety (DFT: 42.3°; HF: 47.3°; X-ray: 50.3°).

Fig. 10 summarises the B3P86-optimised geometry calculated for **9** together with those obtained for its molecular constituents. Selected bond lengths are included in Table 1. The optimised parameters are in excellent agreement with X-ray data, the average deviation between theory and experiment is only 0.004 Å for the bond lengths and 0.6° for the bond angles. The bond lengths and bond angles calculated for the thiophene and quinoxaline moieties of **9** are, with very small deviations, identical to those obtained for the respective isolated molecules, indicating that these moieties preserve their structural identity in **9**. This is not however the case for the

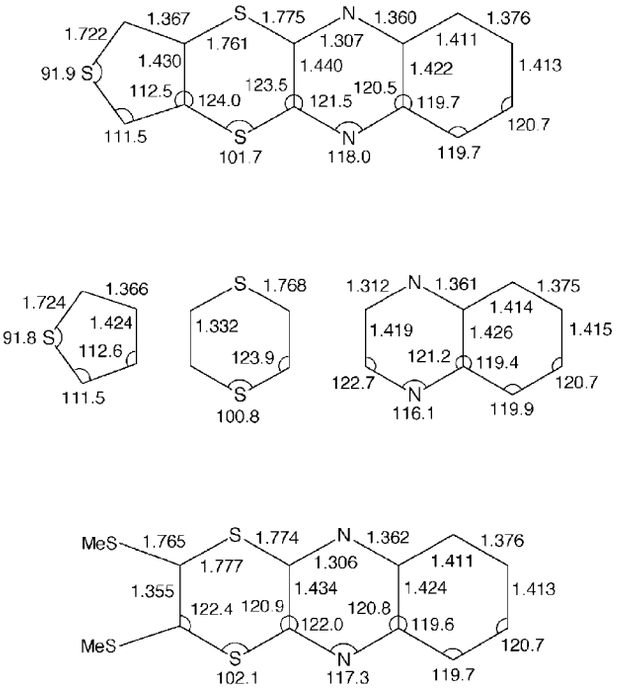

Fig. 10 B3P86/6-31G*-optimised geometries for **9** (C_s symmetry), its molecular components thiophene (C_{2v}), 1,4-dithiine (C_{2v}, boat) and quinoxaline (C_{2v}) and **16** (C_s). Bonds are in Å and angles in degrees.

central dithiine ring, for which the lateral C(2)–C(3) and C(13)–C(14) bonds lengthen from 1.332 Å in the 1,4-dithiine molecule to 1.440 and 1.430 Å in **9**. They therefore lose the highly localised, double-bond character they have in 1,4-dithiine. From the structural standpoint, compound **9** has to be visualised, therefore, as a quinoxaline unit and a thiophene unit linked together by two sulfur bridges and not as a 1,4-dithiine derivative. As discussed below, these structural trends strongly influence the electronic structure and have important consequences on the electrochemical properties.

Fig. 10 also displays the optimised geometry of compound

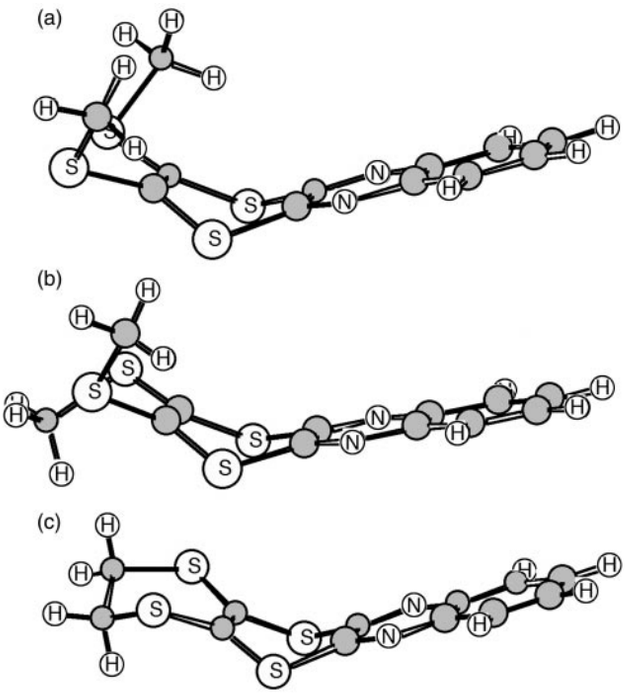

Fig. 11 B3P86/6-31G*-optimised minimum-energy conformations calculated for: a) **16** (C_s), b) **16** (second energy-minimum) and c) **17**.

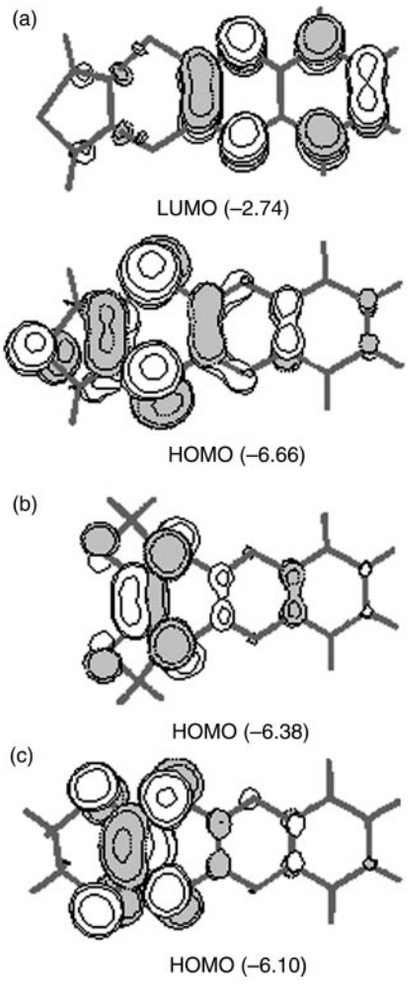

Fig. 12 Electronic density contours calculated for the frontier MOs of (a) **9**, (b) **16** and (c) **17**. The energies of the MOs, in eV, calculated at the B3P86/6-31G* level are included within parentheses.

16. The molecular structure of **16** is intermediate between that of 1,4-dithiine and that of **9**. On the C(4)–C(4′) side (atom numbering from Fig. 9), the quinoxaline unit preserves its structure as in **9**. On the C(5)–C(5′) side, the bond keeps its double-bond character as in 1,4-dithiine. Identical trends are calculated for compound **17**.

In agreement with the X-ray structure, the minimum-energy conformation of **16** corresponds to a C_s structure where both thiomethyl groups point upwards (see Fig. 11a). A second energy minimum, in which SCH_3 groups point in opposite directions (Fig. 11b), is found to lie only 1.00 kcal mol^{-1} higher in energy. This small energy difference was confirmed at the HF/6-31G* level (0.82 kcal mol^{-1}l) and by performing single-point MP2/6-31G* calculations (1.00 kcal mol^{-1}). Both conformations should therefore be present in solution at room temperature (% ratio $\approx$ 85 : 15). For the C_s conformer, the planarisation of the dithiine moiety now costs 3.62 kcal mol^{-1}, twice the value obtained for **9** (1.79 kcal mol^{-1}). The folding of the dithiine ring along the S(1)$\cdots$S(1′) axis in **16** (48.0°) is indeed larger than that found for **9** (42.3°). The calculated value overestimates the X-ray value (40.5°), suggesting that in the crystal of **16** packing forces tend to reduce the folding of the molecules, which is in contrast to that observed for **9**. As discussed above, this feature is due to the thiomethyl groups which, in the crystal structure, interact with the quinoxaline moiety of a neighbour molecule. The twisting of the SCH_3 groups in the crystal (47.4°) is in fact smaller than that calculated for the isolated molecule (58.9°).

Fig. 11c shows the minimum-energy conformation calculated for compound **17**. The folding angle of the dithiine ring along the S$\cdots$S axis has an average value of 48.6°, similar to that found for **16** (48.0°). The outer -SCH_2CH_2S- unit is twisted around the C–C bond in a staggered conformation (60.0°) to avoid the interaction between the hydrogen atoms. The planarisation of the dithiine ring to obtain a C_2 structure, in which the –CH_2CH_2– bond preserves the staggered conformation, now costs 5.39 kcal mol^{-1}.

Fig. 12 sketches the atomic orbital (AO) composition of the highest occupied molecular orbital (HOMO) and lowest unoccupied molecular orbital (LUMO). The HOMO of **9** is mainly localised on the dithiine ring with important contributions from the thiophene and quinoxaline units. The LUMO of **9** (−2.74 eV) spreads over the quinoxaline moiety and corresponds to the LUMO of quinoxaline (−2.58 eV). The MO distributions calculated for compounds **16** and **17** are slightly different from that obtained for **9**. While the LUMO exactly corresponds to that of quinoxaline, as discussed for **9**, the HOMO is mainly located on the $S_2C(5)=C(5')S_2$ environment with negligible contributions from the quinoxaline moiety.

For **9**, the topology of the HOMO suggests that, in a first approach, the electrons extracted upon oxidation are mainly removed from the sulfur bridges, with a large involvement of the thiophene and quinoxaline units. Compared with 1,4-dithiine, for which the HOMO is located at −6.15 eV, the HOMO of **9** (−6.66 eV) is stabilised by 0.51 eV. This stabilisation supports the more positive oxidation potentials measured for **9** (1.60 V *vs* Ag/AgCl) compared with 1,4-dithiine (0.69 V *vs.* SCE).[10] In going to compounds **16** and **17** the energy of the HOMO increases to −6.38 and −6.10 eV, respectively. The HOMO energies thus suggest that compound **17** should undergo oxidation more easily than **16** and **16** more easily than **9**. This MO-based trend does not justify, however, the experimental observations ($E_{ox,1}$ **16**: +1.2 V < **17**: +1.3 V < **9**: +1.6 V) and a more quantitative approach is used below. The topology of the LUMO clearly indicates that the electron introduced upon reduction is added to the quinoxaline unit. The energy of the LUMO lowers in passing from quinoxaline (−2.58 eV) to **9** (−2.74 eV), **16** (−2.85 eV) or **17** (−2.79 eV), supporting the anodic shift experimentally observed for the reduction potential (quinoxaline: −1.80 V,[16] **9**: −1.45 V).

Charged compounds. To get a deeper understanding of the oxidation and reduction processes, the molecular geometries of the radical cation, dication and radical anion of **9** were optimised at both the B3P86 and HF levels. The B3P86 values calculated for the most relevant bond lengths of these species are given in Table 1 to be compared with those obtained for the neutral molecule and with X-ray data.

The oxidation process mainly affects the dithiine environment as suggested above on the basis of the AO composition of the HOMO. The main effect is certainly the planarisation of the dithiine ring and thereby of the molecule, which is already achieved for the radical cation after the extraction of the first electron. Planarisation is accompanied by the shortening of the S(2)–C(2) [S(3)–C(3)] and S(2)–C(13) [S(3)–C(14)] bonds, which reduce their lengths from 1.775 and 1.761 Å for **9** to 1.718 and 1.706 Å for $\mathbf{9}^{2+}$, and, to a lesser degree, by the lengthening of the C(2)–C(3) (0.016 Å) and C(13)–C(14) (0.041 Å) bonds. As can be seen from Table 1, the bond lengths of the *A* and *B* molecules of **9** in the TCNQ complex are somewhat between the values obtained for neutral and singly-oxidised states. This feature, together with the almost planar structure of the donor molecules in the TCNQ complex, suggests a certain degree of charge transfer in contrast with the lack of charge transfer inferred above on the basis of the geometry of the TCNQ molecules.

The structural changes calculated for **9** upon oxidation suggest a gain in aromaticity similar to that found for 1,4-

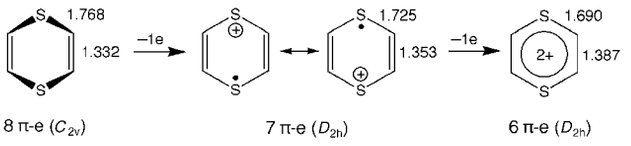

Fig. 13 Evolution upon oxidation of the molecular structure of 1,4-dithiine calculated at the B3P86/6-31G* level. Bond lengths are in Å.

dithiine in passing from the neutral molecule to the dication. As sketched in Fig. 13, the boat C_{2v} structure obtained for neutral 1,4-dithiine (8 π-electrons) evolves to a fully aromatic, planar D_{2h} structure for the dication (6 π-electrons). The gain in aromaticity justifies the low value of the first oxidation potential reported for 1,4-dithiine (+0.69 V)[10] and accounts for the close occurrence of the second oxidation potential (+0.80 V) due to the high stability of the dication. The case of **9** is indeed drastically different. On the one hand, **9** is already constituted by two aromatic units, thiophene with 6 π-electrons and quinoxaline with 10 π-electrons. On the other hand, these units largely participate in the oxidation process. In going to the cation, 0.46 e are extracted from the sulfur bridges S(2) and S(3), 0.30 e from the quinoxaline unit and 0.24 e from the thiophene ring. For the dication, the extracted charges are 0.81, 0.69 and 0.50 e, respectively. The whole molecule is thus oxidised and the gain in aromaticity, although $\mathbf{9}^{2+}$ is an 18 π-electron system, is not comparable to that obtained for 1,4-dithiine. The greater relative stability of the cation of 1,4-dithiine justifies the large anodic shift measured for the first oxidation potential in passing from 1,4-dithiine (0.69 V)[10] to **9** (1.60 V).

Molecules **16** and **17** were also calculated in oxidised and reduced states for comparison purposes. The presence of the methylthio and ethylenedithio substituents determines a significant difference with respect to compound **9**, because they largely participate in the oxidation process. Now, the molecular environment defined by the five bonds in between the four sulfur atoms ($S_2C{=}CS_2$) undergoes the most important

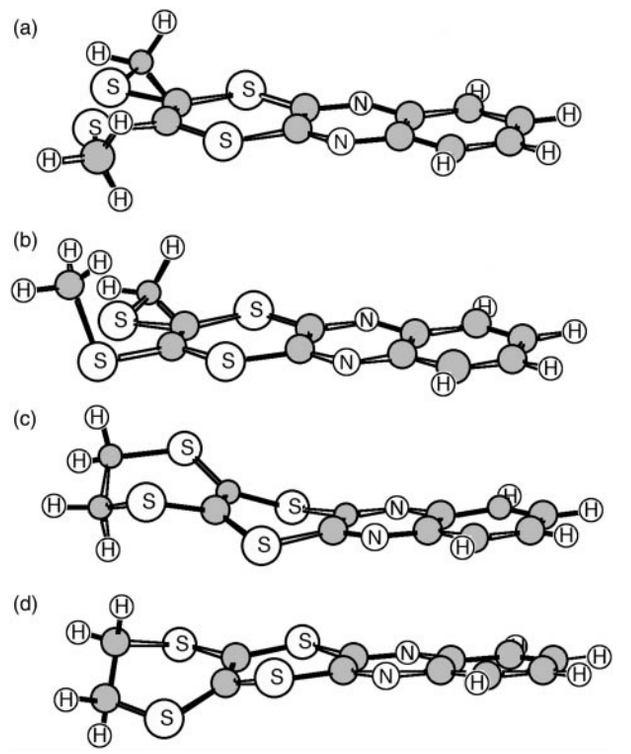

Fig. 14 B3P86/6-31G*-optimised minimum-energy conformations calculated for: a) $\mathbf{16}^{+}$ (C_{2v}), b) $\mathbf{16}^{+}$ (C_1, second energy-minimum), c)$\mathbf{17}^{+}$ and d) $\mathbf{17}^{2+}$.

changes upon oxidation. In going from neutral **16** to $\mathbf{16}^{2+}$, the C(5)–C(5′) bond lengthens from 1.355 to 1.468 Å and the C(5)–S(2) [C(5′)–S(2′)] and C(5)–S(1) [C(5′)–S(1′)] bonds shorten from 1.777 to 1.713 Å and from 1.774 to 1.703 Å, respectively. By contrast to that found for **9**, the S(1)–C(4) [S(1′)–C(4′)] bond only undergoes a small shortening of 0.020 Å from 1.774 to 1.754 Å. Identical trends are obtained for **17**. The rationale behind these changes is that for **16** and **17** charge is mainly extracted from the $S_2C{=}CS_2$ environment. For instance, 1.54 e are extracted for $\mathbf{16}^{2+}$ from that environment and the remaining 0.46 e from the quinoxaline unit.

As for **9**, oxidation induces the planarisation of **16**, for which a fully planar C_{2v} structure is obtained for the cation as the most stable conformation (Fig. 14a). A second energy minimum (Fig. 14b), in which one SCH_3 group lies in the plane of the molecule and the other lies perpendicular to the molecule, is found 3.82 kcal mol^{-1} higher in energy (HF: 1.74 kcal mol^{-1}; MP2: 1.52 kcal mol^{-1}). Force calculations were performed to confirm the energy-minimum character of this structure. The dication maintains the planar C_{2v} structure as the most stable conformer. By contrast to **9** and **16**, the cation and dication of **17** are not planar (see Fig. 14c and 14d). For $\mathbf{17}^{+}$, the dithiine ring is bent along the S···S axis by an average angle of 29.8°, preserving some of the folding observed for the neutral molecule (48.7°). For $\mathbf{17}^{2+}$, the molecule presents a rotation angle of 20.2° around the $S_2C{=}CS_2$ bond, which has lengthened from 1.348 (**17**) to 1.445 Å ($\mathbf{17}^{2+}$) making possible such rotation. For both species the terminal CH_2–CH_2 group adopts a staggered conformation, thus minimising the steric interactions.

The lack of planarity for $\mathbf{17}^{+}$ and $\mathbf{17}^{2+}$ indicates that these species are relatively less stable than the cations of **16**. The ionisation energies calculated for **17** ($E_{\text{cation}}-E_{\text{neutral}}=7.45$ eV, $E_{\text{dication}}-E_{\text{cation}}=11.59$ eV) are higher than those obtained for **16** (7.31 and 11.20 eV). This explains the higher oxidation potentials recorded for **17** compared to **16**, a result that could not be rationalised on the basis of HOMO energies. The ionisation energies of **16** and **17** are lower than those computed for **9** (7.84 and 12.12 eV), in accordance with the significantly higher oxidation potentials found for **9**.

The analysis of the structural changes calculated upon oxidation has been very useful in rationalising the relative values of the oxidation potentials but give no answer to the irreversible behaviour experimentally observed for the oxidation processes in **9** (Fig. 1). The planarisation of **9** cannot be invoked to explain this irreversibility, since it also takes place for 1,4-dithiine and other related systems such as thianthrene derivatives, for which the two oxidation waves to the dication are fully reversible.[10,22] We have, however, disregarded an important electronic feature of **9** when calculating the dication. The second electron has been considered to be removed from the same MO as the first electron (*i.e.*, from the HOMO) and a closed-shell singlet dication has been assumed to result from the second oxidation process. This is fully justified for most donor molecules since the HOMO lies well-above the remaining occupied MOs. For instance, the HOMO of 1,4-dithiine (−6.15 eV) lies 2.0 eV above the HOMO−1 (−8.16 eV). This is not however the case for compound **9**, for which only 0.25 eV separate the HOMO (−6.66 eV) and HOMO−1 (−6.91 eV).

The dication of **9** was, therefore, recalculated assuming that electrons are extracted from different MOs. The B3P86 method converged to a triplet state in which one electron is removed from the HOMO and the other electron from the HOMO−1. The triplet state is more stable than the closed-shell singlet state by only 0.04 eV. This difference is too small to conclude unambiguously that the fundamental state of $\mathbf{9}^{2+}$ is a triplet. Nevertheless, the attainment of this highly reactive species in the second oxidation process should be considered as a possible explanation for the high irreversibility observed in the

voltammogram of **9**. In fact, the existence of a triplet state in dicationic 1,4-dithiine species has been previously suggested.[23]

The dications of **16** and **17** were also calculated with a triplet multiplicity to compare with **9**. The situation is different from that found for **9** because the HOMO and HOMO−1 are now separated by 0.71 (**16**) and 1.18 eV (**17**). As a consequence, the triplet state is calculated to lie 0.75 (**16**) and 0.42 eV (**17**) above the singlet state and relatively stable closed-shell dications should therefore be expected in the second oxidation process for **16** and **17**.

In the search for theoretical support for the square diagram depicted in Fig. 3, the cation of this derivative was reinvestigated at the B3P86/6-31G* in the presence of the solvent (dichloromethane). Taking the C_s structure of the neutral molecule as the starting point, the geometry of $\mathbf{16}^+$ was reoptimised using different self-consistent reaction fields (SCRF) models to simulate the solvent. In all cases, the cation evolved to the C_{2v} planar structure depicted in Fig. 14a and no nonplanar energy minimum was found for $\mathbf{16}^+$. The nonplanar intermediate $\mathbf{16}^+_A$ suggested in Fig. 3 is therefore not located as a stationary point in the potential energy hypersurface.

A second plausible explanation for the anodic behaviour of **16** comes from theoretical calculations, just taking into account that two minima are actually predicted for $\mathbf{16}^+$, *viz.* the C_{2v} and C_1 structures depicted in Fig. 14a and 14b. The $C_1 \rightarrow C_{2v}$ interconversion by rotation of the methyl group around the S(2′)–C(5′) bond is calculated to be restricted by a barrier of only a few tenths of kcal mol^{-1} (HF: 0.3 kcal mol^{-1}; DFT: 0.1 kcal mol^{-1}). At slow scan rates, the conversion $C_1 \rightarrow C_{2v}$ is approximately at its equilibrium and the most stable C_{2v} structure predominates. The oxidation of this structure to obtain the C_{2v} dication of **16** gives rise to the second oxidation potential at *ca.* +1.6 V. As the scan rate is increased, the concentration of the C_1 species increases and the signal at +1.5 V represents the oxidation of this system. Structures C_1 and C_{2v} thus can play the role of species $\mathbf{16}^+_A$ and $\mathbf{16}^+_B$ in Fig. 3. The difference in the oxidation potentials of these structures is due to the higher stability of the C_{2v} conformation. In the presence of the solvent (CH_2Cl_2), the energy difference calculated between the C_1 and C_{2v} structures at the B3P86 level is 2.94 kcal mol^{-1} (0.13 eV).

We finally discuss the reduction process taking **9** as a representative example. As suggested above on the basis of the AO composition of the LUMO, the introduction of one extra electron mainly affects the quinoxaline unit, which incorporates an extra charge of −0.65 e in the anion. The largest structural modifications (see Table 1) are obtained for the C(2)–C(3) bond, which shortens by 0.054 Å due to the bonding nature it shows in the LUMO (see Fig. 12), and for the N(1)–C(2) and N(4)–C(3) bonds, which lengthen by 0.038 Å due to their antibonding character. The dithiine ring remains folded upon reduction, the bending angle along the S···S axes being enlarged to 45.3°. Identical trends are obtained for **16** and **17**. The electron affinities, calculated as the energy differences between the total energies of the neutral molecules and the anions, are 1.32 (**9**), 1.45 (**16**) and 1.37 eV (**17**). These values are 0.5–0.6 eV larger than that obtained for the quinoxaline molecule (0.79 eV) justifying the better acceptor properties (*i.e.*, the less negative reduction potentials) found for the 1,4-dithiinoquinoxaline derivatives studied here.

Conclusion

We have presented the syntheses of a short series of dithiinoquinoxaline derivatives, which exhibit varied and interesting redox properties. The subtle changes in the chemical structure of these compounds, particularly between **16** and **17**, result in a striking difference in electrochemical behaviour. X-Ray crystallography of **9**·TCNQ reveals the donor molecule as a highly delocalised π-electron planar system, which is in contrast to the bowed structure of the neutral species. The electrochemical properties and molecular geometries of the dithiinoquinoxaline derivatives have been modelled using HF and DFT calculations; we have found that there is a strong correlation between our experimental and theoretical results. Although **9**·TCNQ is an insulator, the structural change in oxidation states is an important criterion for the development of potentially conducting materials.

Experimental

General

Melting points were taken using Electrothermal melting point apparatus and are uncorrected. ^{1}H and ^{13}C NMR spectra were recorded on a Bruker AC 250 instrument; chemical shifts are given in ppm; all *J* values are in Hz. IR spectra were recorded on a Mattson Genesis Series FTIR spectrometer. Mass spectra (EI) and high resolution mass spectra were recorded on a 7070E VG analytical mass spectrometer. Elemental analyses were obtained by MEDAC Ltd.

Cyclic voltammetry

The measurements for compounds **9**, **16** and **17** were performed on a BAS CV50W voltammetric analyser with *iR* compensation, using anhydrous dichloromethane as the solvent, Ag/AgCl as the reference electrode and platinum wire and platinum disk (1.6 mm diameter) as the counter and working electrodes, respectively. All solutions were degassed (N_2) and contained the substrate in concentrations *ca.* 10^{-4} M, together with Bu_4NPF_6 (0.1 M) as the supporting electrolyte.

X-Ray crystallography

Pale yellow parallelepipedal crystals of **9** were grown from dichloromethane–ethanol, black needle-like crystals of **9**·TCNQ from acetonitrile. The diffraction from **9**·TCNQ was extremely weak, with relatively high diffuse scattering. The difference Fourier map of **9**·TCNQ shows high level of residual (diffuse) electron density, up to 1 eÅ^{-3}, extending from the molecules in longitudinal directions and coplanar with them. A second X-ray study on a different crystal (at $T = 150$ K, final $R = 0.087$) revealed the same features. The structure solution and refinement in the non-centrosymmetric space group *P*1 did not solve the problem, which is probably due to a systematic twinning or incommensurate disorder which we could not rationalise.

Compound **16** was recrystallised from ethyl acetate–petroleum ether to afford orange cubic crystals. Data were collected on a $0.7 \times 0.5 \times 0.4$ mm crystal and no absorption correction applied as refined parameters were acceptable, with the residual electron density = 0.29 and −0.38 eÅ^{-3}.

All structures were solved *via* direct methods and refined against F^2 using the SHELXL-97[24] suite of programs. All non-H atoms were refined anisotropically whilst hydrogens were treated isotropically in calculated, 'riding' model positions.

Crystal data and experimental details are listed in Table 3, the full structural data (excluding structure factors) have been deposited with the Cambridge Crystallographic Data Centre; CCDC reference number 1145/242. See http://www.rsc.org/suppdata/jm/b0/b003910l/ for crystallographic files in .cif format.

Computational methods

The calculations were performed using the Gaussian 94[25] and Gaussian 98[26] systems of programs on SGI-ORIGIN 2000 computers at the Departamento de Química Física and at the

Table 3 Crystal data

Compound	**9**	**16**	**9**·TCNQ
Formula	$C_{12}H_6N_2S_3$	$C_{12}H_{10}N_2S_4$	$C_{12}H_6N_2S_3^+$ $C_{12}H_4N_4^-$
Formula weight	274.4	310.46	478.6
T /K	150	293	120
Crystal system	Triclinic	Orthorhombic	Triclinic
Space group	$P\bar{1}$ (#2)	*Pnma* (#62)	$P\bar{1}$ (#2)
a/ Å	6.876(2)	9.5292(14)	8.059(1)
b/Å	9.361(3)	10.2412(6)	12.144(1)
c/ Å	9.508(4)	13.975(2)	22.257(2)
α/ °	101.96(1)	90.0	76.95(1)
β/°	95.96(1)	90.0	85.24(1)
γ/ °	104.09(1)	90.0	79.67(1)
V/ Å^3	573.0(2)	1363.8(3)	2085.6(4)
Z	2	4	4
μ/ mm^{-1}	0.62	0.678	0.38
Reflections measured	3221	5060	11556
Unique reflections	1786	1123	7307
R_{int}	0.033	0.124	0.116
$R[F^2 > 2\sigma(F^2)]$	0.029	0.044	0.068
$R(F^2)$, all data	0.082	0.052	0.193

Servei de Informàtica of the University of Valencia. Geometry optimisations were carried out at the Hartree–Fock (HF) and density functional theory (DFT) levels using the split-valence, double-ζ polarised 6-31G* basis set[27] and the hybrid, gradient-corrected B3P86 density functional.[28] The geometries of neutral molecules and dications were computed within the restricted Hartree–Fock (RHF) formalism. The spin-unrestricted Hartree–Fock (UHF)[29] approximation, in which electrons with different spins occupy different sets of orbitals, was used for singly charged cations and to calculate dications in triplet states. No significant spin contamination was obtained in the calculations for open-shell systems. The Berny analytical method[30] was employed for the optimisations and the threshold values for the maximum force and the maximum displacement were 0.00045 and 0.0018 au, respectively. Additional single-point calculations were done for compound **16** at the second-order Møller–Plesset (MP2) perturbation theory level[31] over B3P86 fully-optimised geometries. Geometry optimisations including solvent effects were carried out using the self-consistent reaction field (SCRF) approach and the Onsanger[32] and polarised continuum (PCM)[33] models to simulate the solvent. Both models led to the same results for $\mathbf{16}^{+}\cdot$. An attempt was made to perform more elaborated SCI-PCM[34] calculations, where the cavity in which the solute is placed is determined self-consistently from an isodensity surface, but convergence was not reached due to the large size of the considered molecules.

General procedure for compounds 9, 16 and 17

To a stirred solution of the corresponding [1,3]dithiol-2-one (**10**, **12** or **13**) in ethanol (*ca.* 50 mL), at 0 °C, was added NaOEt (2 equivalents from a freshly prepared 1.5–2.0 M ethanolic solution). After stirring the reaction at 0 °C for 45 min, ether was added (200 mL) and the precipitate was filtered under nitrogen using a sintered Schlenk tube. The solid was washed with ether (2 × 25 mL) and dissolved in THF (200 mL). After the addition of 2,3-dichloroquinoxaline (*ca.*1 equivalent), the reaction was allowed to stir for 16 h. The solvent was evaporated under reduced pressure and the residue was column chromatographed using silica gel and ethyl acetate–petroleum ether (1 : 5) as the eluent. The products were recrystallised from dichloromethane–ethanol (**9**) or petroleum ether–ethyl acetate (**16** and **17**).

Thieno[3′,4′ : 5,6][1,4]dithiino[2,3-*b*]quinoxaline (9)

Using 1.50 g (8.62 mmol) of compound **10** and 1.75 g of 2,3-dichloroquinoxaline (8.79 mmol), a pale yellow crystalline solid was obtained (1.00 g, 42% yield); mp 161–163 °C (Found C, 52.4; H, 2.1; N, 10.2. $C_{12}H_6N_2S_3$ requires C, 52.5; H, 2.2; N, 10.2%); *m*/*z* (EIMS) 274; ^{1}H NMR (250 MHz, $CDCl_3$) δ 7.90 (2H, dd, *J* 6.3 and 3.5), 7.67 (2H, dd, *J* 6.4 and 3.4) and 7.27 (2H, s); ^{13}C NMR (250 MHz, $CDCl_3$) δ 152.2, 140.4, 130.5, 128.5, 127.7 and 121.4; ν_{max}/cm^{-1} (KBr) 3055, 1257, 1177, 1109, 1013, 828, 763, 598 and 436.

2,3-Bis(methylsulfanyl)[1,4]dithiino[2,3-*b*]quinoxaline (16)

Using 5.6 g (26.67 mmol) of compound **12** and 5.40 g of 2,3-dichloroquinoxaline (27.14 mmol), a yellow crystalline solid was obtained (4.55 g, 55% yield); mp 154–155 °C (Found C, 46.4; H, 3.2; N, 9.1. $C_{12}H_{10}N_2S_4$ requires C, 46.4; H, 3.3; N, 9.0%); *m*/*z* (EIMS) 310; HRMS (M^+) 309.97322, calculated for $C_{12}H_{10}N_2S_4$ 309.97269; ^{1}H NMR (250 MHz, $CDCl_3$) δ 7.90 (2H, dd, *J* 6.3 and 3.5), 7.67 (2H, dd, *J* 6.4 and 3.5) and 2.52 (6H, s); ^{13}C NMR (250 MHz, $CDCl_3$) δ 153.0, 141.3, 130.7, 128.8, 127.2 and 19.1; ν_{max}/cm^{-1} (KBr) 1414, 1336, 1263, 1180, 1115, 852, 763, and 596.

2,3-Ethylenedisulfanyl[1,4]dithiino[2,3-*b*]quinoxaline (17)

Using 4.0 g (19.23 mmol) of compound **13** and 3.90 g of 2,3-dichloroquinoxaline (19.60 mmol), a brown solid was obtained (2.84 g, 48% yield); mp 156–158 °C (Found C, 46.8; H, 2.7; N, 9.0. $C_{12}H_8N_2S_4$ requires C, 46.7; H, 2.6; N, 9.1%); *m*/*z* (EIMS) 308; ^{1}H NMR (250 MHz, $CDCl_3$) δ 7.96 (2H, dd, *J* 6.3 and 3.4), 7.71 (2H, dd, *J* 6.3 and 3.4) and 3.32 (4H, s); ^{13}C NMR (250 MHz, $CDCl_3$) δ 153.4, 141.1, 130.8, 128.9, 118.1 and 32.0; ν_{max}/cm^{-1} (KBr) 1523, 1259, 1176, 1111, 989, 757, 650, 596 and 523.

Thieno[3′,4′ : 5,6][1,4]dithiino[2,3-*b*]quinoxaline–tetracyano-*p*-quinodimethane charge-transfer complex (9·TCNQ)

To a refluxing solution of **9** (100 mg, 0.36 mmol) in dry dichloromethane (10 mL), was added a warm solution of 7,7,8,8-tetracyanoquinodimethane (75 mg, 0.37 mmol). The mixture was refluxed for 10 min and allowed to cool to room temperature. After slow evaporation of the solvent over several days, dark green crystals of the complex **9**·TCNQ were deposited (30 mg), which were filtered and washed with cold dichloromethane.

(Found C, 56.0; H, 2.2; N, 14.0. $C_{48}H_{22}N_{10}S_9$ (3 : 1 complex) requires C, 56.1; H, 2.2; N, 13.6%);ν_{max}/cm^{-1} (KBr) 3104, 2217 (CN), 1540, 1177, 1115, 840, 790, 773 and 469.

Acknowledgements

We thank the Royal Society for equipment related to cyclic voltammetry (PJS). Financial support from Spanish DGES-MEC under grants PB95-0428-C02-02 ,PB98-1447 and 1FD97-1765-C03-01 is gratefully acknowledged by the group of Valencia.

References

1 Recent reviews: M. R. Bryce, *Chem. Soc. Rev.*, 1991, **20**, 355; J. M. Williams, J. R. Ferraro, R. J. Thorn, K. D. Carlson, U. Geiser, H. H. Wang, A. M. Kini and M.-H. Whangbo, *Organic Superconductors (Including Fullerenes); Synthesis, Structure, Properties and Theory*, Prentice Hall, Englewood Cliffs, NJ, 1992; M. R. Bryce, *J. Mater. Chem.*, 1995, **5**, 1481; M. J. Rosseinsky, *J. Mater. Chem.*, 1995, **5**, 1497; K. Tanigaki and K. Prassides, *J. Mater. Chem.*, 1995, **5**, 1515; P. Cassoux, *Coord. Chem. Rev.*, 1999, **185–186**, 213; D. V. Konarev, R. N. Lyubovskaya, N. V. Drichko, E. I. Yudanova, Y. M. Shul'ga, A. L. Litvinov, V. N. Semkin and B. P. Tarasov, *J. Mater. Chem.*, 2000, **10**, 803.
2 K. Nakasuji, *Pure Appl. Chem.*, 1990, **62**, 477.
3 M. R. Bryce, *J. Mater. Chem.*, 2000, **10**, 589.
4 E. Aqad, J. Y. Becker, J. Bernstein, A. Ellern, V. Khodorkovsky and L. Shapiro, *J. Chem. Soc., Chem. Commun.*, 1994, 2775.
5 K. S. Varma, S. Edge, A. E. Underhill, J. Becher and G. Bojesen, *J. Chem. Soc., Perkin Trans. 1*, 1990, 2563.
6 M. R. Bryce, A. Chesney, A. K. Lay, A. S. Batsanov and J. A. K. Howard, *J. Chem. Soc., Perkin Trans. 1*, 1996, 2451.
7 M. R. Bryce, A. K. Lay, A. Chesney, A. S. Batsanov, J. A. K. Howard, U. Buser, F. Gerson and P. Merstetter, *J. Chem. Soc., Perkin Trans. 2*, 1999, 755.
8 M. Matsuoka, A. Iwamoto, N. Furukawa and T. Kitao, *J. Heterocycl. Chem.*, 1992, **29**, 439.
9 B. Bueno, B. Esteve, J. Irurre, E. Brillas, X. Torrelles, J. Rius, A. Alvarez-Larena, J. F. Piniella, C. Alemán and L. Juliá, *J. Chem. Soc., Perkin Trans. 2*, 1999, 1503.
10 K. Kobayashi and C. L. Gajurel, *Sulfur Rep.*, 1986, **7**, 123.
11 E. Demiralp and W. A. Goddard III, *Synth. Met.*, 1995, **72**, 297; E. Demiralp, S. Dasgupta and W. A. Goddard III, *J. Am. Chem. Soc.*, 1995, **117**, 8154; E. Demiralp and W. A. Goddard III, *J. Phys. Chem.*, 1997, **101**, 8128.
12 L. Chiang, P. Shu, D. Holt and D. Cowan, *J. Org. Chem.*, 1983, **48**, 4713.
13 K. Hartke, T. Kissel, J. Quante and R. Matusch, *Chem. Ber.*, 1980, **113**, 1898.
14 For the electropolymerisation of **9**, see following paper; L. M. Goldenberg, P. J. Skabara, D. M. Roberts, R. Berridge, E. Ortí, P. M. Viruela and R. Pou-Amérigo, *J. Mater. Chem.*, 2000, DOI: 10.1039/b003914o.
15 J. Heinze, *Angew. Chem., Int. Ed. Engl.*, 1993, **32**, 1268.
16 B. J. Tabner and J. R. Yandle, *J. Chem. Soc., A*, 1968, 381.
17 J. Roncali, *Chem. Rev.*, 1992, **92**, 7069.
18 Yu. V. Zefirov and P. M. Zorkii, *Russ. Chem. Rev.*, 1995, **64**, 415; S. Rowland and R. Taylor, *J. Phys. Chem.*, 1996, **100**, 7384.
19 T. J. Kistenmacher, T. J. Emge, A. N. Bloch and D. O. Cowan, *Acta Crystallogr., Sect. B*, 1977, **38**, 1193.
20 W. E. Broderick, J. A. Thompson, E. P. Day and B. M. Hoffman, *Science*, 1990, **249**, 401; D. Stein, H. Sitzmann and R. Böse, *J. Organomet. Chem.*, 1991, **421**, 275; E. Cerrada, M. C. Gimeno, A. Laguna, M. Laguna, V. Orrera and P. G. Jones, *J. Organomet. Chem.*, 1996, **506**, 203.
21 P. A. Howell, R. M. Curtis and W. W. Lipscomb, *Acta Crystallogr.*, 1954, **7**, 498.
22 H. Bock, R. Rauschenbach, K. Ruppert and Z. Havlas, *Angew. Chem., Int. Ed. Engl.*, 1991, **30**, 714.
23 T. Nishinaga, A. Wakamiya and K. Komatsu, *Chem. Commun.*, 1999, 777.
24 G. M. Sheldrick, SHELXL-97. Program for the refinement of crystal structures, University of Göttingen, 1997.
25 M. J. Frisch, G. W. Trucks, H. B. Schlegel, P. M. W. Gill, B. G. Johnson, M. A. Robb, J. R. Cheeseman, T. Keith, G. A. Petersson, J. A. Montgomery, K. Raghavachari, M. A. Al-Laham, V. G. Zakrzewski, J. V. Ortiz, J. B. Foresman, J. Cioslowski, B. B. Stefanov, A. Nanayakkara, M. Challacombe, C. Y. Peng, P. Y. Ayala, W. Chen, M. W. Wong, J. L. Andres, E. S. Replogle, R. Gomperts, R. L. Martin, D. J. Fox, J. S. Binkley, D. J. Defrees, J. Baker, J. P. Stewart, M. Head-Gordon, C. Gonzalez and J. A. Pople, GAUSSIAN 94, Revision D.3, Gaussian, Inc., Pittsburgh PA, 1995.
26 M. J. Frisch, G. W. Trucks, H. B. Schlegel, G. E. Scuseria, M. A. Robb, J. R. Cheeseman, V. G. Zakrzewski, J. A. Montgomery Jr., R. E. Stratmann, J. C. Burant, S. Dapprich, J. M. Millam, A. D. Daniels, K. N. Kudin, M. C. Strain, O. Farkas, J. Tomasi, V. Barone, M. Cossi, R. Cammi, B. Mennucci, C. Pomelli, C. Adamo, S. Clifford, J. Ochterski, G. A. Petersson, P. Y. Ayala, Q. Cui, K. Morokuma, D. K. Malick, A. D. Rabuck, K. Raghavachari, J. B. Foresman, J. Cioslowski, J. V. Ortiz, B. B. Stefanov, G. Liu, A. Liashenko, P. Piskorz, I. Komaromi, R. Gomperts, R. L. Martin, D. J. Fox, T. Keith, M. A. Al-Laham, C. Y. Peng, A. Nanayakkara, C. Gonzalez, M. Challacombe, P. M. W. Gill, B. Johnson, W. Chen, M. W. Wong, J. L. Andres, C. Gonzalez, M. Head-Gordon, E. S. Replogle and J. A. Pople, GAUSSIAN 98, Revision A.6, Gaussian, Inc., Pittsburgh PA, 1998.
27 P. C. Hariharan and J. A. Pople, *Chem. Phys. Lett.*, 1972, **16**, 217.
28 The B3P86 functional consists of Becke's three-parameter hybrid functional,[28a] which is a hybrid of Hartree–Fock exchange with local and gradient-corrected exchange and correlation terms, with the nonlocal correlation provided by the "Perdew 86[28b] expression.
28 A. D. Becke, *J. Chem. Phys.*, 1993, **98**, 5648.
28 J. P. Perdew, *Phys. Rev. B*, 1986, **33**, 8822.
29 J. A. Pople and R. K. Nesbet, *J. Chem. Phys.*, 1954, **22**, 571.
30 H. B. Schlegel, *J. Comput. Chem.*, 1982, **3**, 214.
31 C. Møller and M. S. Plesset, *Phys. Rev.*, 1934, **46**, 618; J. S. Binkley and J. A. Pople, *Int. J. Quantum Chem.*, 1975, **9**, 229; R. Krishnan, M. J. Frisch and J. A. Pople, *J. Chem. Phys.*, 1980, **72**, 4244.
32 M. W. Wong, M. J. Frisch and K. B. Wiberg, *J. Am. Chem. Soc.*, 1991, **113**, 4776; M. W. Wong, K. B. Wiberg and M. J. Frisch, *J. Chem. Phys.*, 1991, **95**, 8991.
33 S. Miertus, E. Scrocco and J. Tomasi, *J. Chem. Phys.*, 1981, **55**, 117; R. Cammi and J. Tomasi, *J. Comput. Chem.*, 1995, **16**, 1449; M. Cossi, V. Barone, R. Cammi and J. Tomasi, *Chem. Phys. Lett.*, 1996, **255**, 327.
34 J. B. Foresman, T. A. Keith, K. B. Wiberg, J. Snoonian and M. J. Frisch, *J. Phys. Chem.*, 1996, **100**, 16098.